AD-A146 755 AERO-OPTICS EXPERIMENTAL TECHNIQUES(U) SPECTRON 1/1
DEVELOPMENT LABS INC COSTA MESA CA W C ROSE JUL 84
AFWL-TN-84-30 F29601-82-C-0013

UNCLASSIFIED F/G 20/4 NL

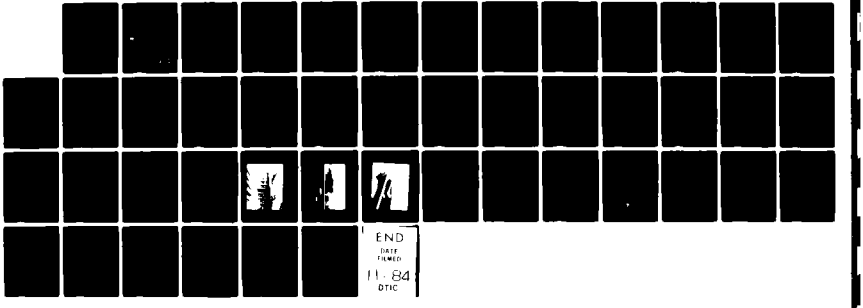

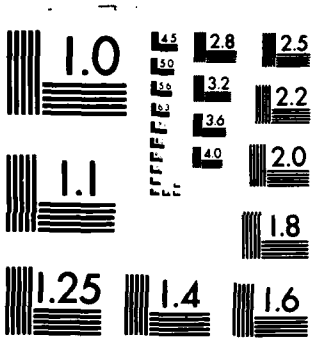

AFWL-TN-
84-30

AERO-OPTICS EXPERIMENTAL TECHNIQUES

W.C. Rose

Rose Engineering & Research, Inc.
Incline Village, NV 89450

July 1984

Final Report

Approved for public release; distribution unlimited.

AIR FORCE WEAPONS LABORATORY
Air Force Systems Command
Kirtland Air Force Base, NM 87117

AFWL-TN-84-30

This final report was prepared by the Spectron Development Laboratories, Inc., Costa Mesa, California under Contract F29601-82-C-0013, Job Order 317J0208 with the Air Force Weapons Laboratory, Kirtland Air Force Base, New Mexico. Captain Francis L. Smith (ARDE) was the Laboratory Project Officer-in-Charge.

When Government drawings, specifications, or other data are used for any purpose other than in connection with a definitely Government-related procurement, the United States Government incurs no responsibility or any obligation whatsoever. The fact that the Government may have formulated or in any way supplied the said drawings, specifications, or other data, is not to be regarded by implication, or otherwise in any manner construed, as licensing the holder, or any other person or corporation; or as conveying any rights or permission to manufacture, use, or sell any patented invention that may in any way be related thereto.

This report has been authored by a contractor of the United States Government. Accordingly, the United States Government retains a nonexclusive, royalty-free license to publish or reproduce the material contained herein, or allow others to do so, for the United States Government purposes.

This report has been reviewed by the Public Affairs Office and is releasable to the National Technical Information Services (NTIS). At NTIS, it will be available to the general public, including foreign nations.

If your address has changed, if you wish to be removed from our mailing list, or if your organization no longer employs the addressee, please notify AFWL/ARDE, Kirtland AFB, NM 87117 to help us maintain a current mailing list.

This technical report has been reviewed and is approved for publication.

Francis L. Smith

FRANCIS L. SMITH
Capt, USAF
Project Officer

FOR THE COMMANDER

Nazareno L. Rapagnani

NAZARENO L. RAPAGNANI
Chief, Fluid Mechanics Branch

Winston K. Pendleton

WINSTON K. PENDLETON
Col, USAF
Ch, Laser Science & Technology Office

DO NOT RETURN COPIES OF THIS REPORT UNLESS CONTRACTUAL OBLIGATIONS OR NOTICE ON A SPECIFIC DOCUMENT REQUIRES THAT IT BE RETURNED.

UNCLASSIFIED

SECURITY CLASSIFICATION OF THIS PAGE

REPORT DOCUMENTATION PAGE

1a. REPORT SECURITY CLASSIFICATION Unclassified	1b. RESTRICTIVE MARKINGS
2a. SECURITY CLASSIFICATION AUTHORITY	3. DISTRIBUTION/AVAILABILITY OF REPORT Approved for public release; distribution unlimited.
2b. DECLASSIFICATION/DOWNGRADING SCHEDULE	
4. PERFORMING ORGANIZATION REPORT NUMBER(S)	5. MONITORING ORGANIZATION REPORT NUMBER(S) AFWL-TN-84-30
6a. NAME OF PERFORMING ORGANIZATION Rose Engineering & Research Inc 6b. OFFICE SYMBOL (If applicable)	7a. NAME OF MONITORING ORGANIZATION Air Force Weapons Laboratory (ARDE)
6c. ADDRESS (City, State and ZIP Code) PO Box 5146 Incline Village NV 89450	7b. ADDRESS (City, State and ZIP Code) Kirtland AFB NM 87117
8a. NAME OF FUNDING/SPONSORING ORGANIZATION 8b. OFFICE SYMBOL (If applicable)	9. PROCUREMENT INSTRUMENT IDENTIFICATION NUMBER. F29601-82-C-0013
8c. ADDRESS (City, State and ZIP Code)	10. SOURCE OF FUNDING NOS. PROGRAM ELEMENT NO. 62605F; PROJECT NO. 317J; TASK NO. 02; WORK UNIT NO. 08
11. TITLE (Include Security Classification) AERO-OPTICS EXPERIMENTAL TECHNIQUES (U)	
12. PERSONAL AUTHOR(S) Rose, W. C.	
13a. TYPE OF REPORT Final Report 13b. TIME COVERED FROM _____ TO _____	14. DATE OF REPORT (Yr., Mo., Day) 1984, July 15. PAGE COUNT 46
16. SUPPLEMENTARY NOTATION	

17. COSATI CODES		
FIELD	GROUP	SUB. GR.
20	04	

18. SUBJECT TERMS (Continue on reverse if necessary and identify by block number)
Hot-wire anemometry, turbulent flow field, pressure probes, shear layers, boundary layers.

19. ABSTRACT (Continue on reverse if necessary and identify by block number)

This report summarizes results of a study to determine the most appropriate aerodynamic experimental techniques for gathering data in aircraft boundary layer and shear layer flow fields. It focuses on two primary techniques: hot-wire anemometry and five-hole pressure probes, and develops reduction equations for obtaining the desired aerodynamic parameters from raw data. It also presents comparisons of hot-wire data using splitfilm probes and x-film probes collected during an airborne experiment.

20. DISTRIBUTION/AVAILABILITY OF ABSTRACT UNCLASSIFIED/UNLIMITED ☐ SAME AS RPT. ☐ DTIC USERS ☒	21. ABSTRACT SECURITY CLASSIFICATION Unclassified
22a. NAME OF RESPONSIBLE INDIVIDUAL Captain Francis L. Smith	22b. TELEPHONE NUMBER (Include Area Code) (505) 844-0208 22c. OFFICE SYMBOL AFWL/ARDE

DD FORM 1473, 83 APR EDITION OF 1 JAN 73 IS OBSOLETE.

UNCLASSIFIED

SECURITY CLASSIFICATION OF THIS PAGE

SECTION I BACKGROUND

Aerodynamic flow fields encountered in AFWL applications range from internal flow within laser cavities to external three-dimensional, turbulent flow fields surrounding beam propagation systems on various aircraft. This wide range and complexity of flow fields dictate proper selection, calibration and use of aerodynamic instrumentation in order to quantify the flow fields for use in determining propagation effects as well as providing a data base for numerical simulations. Two primary areas of advanced aerodynamic instrumentation for use in experimental flow-field diagnostics are considered here. The first is the practical and quantitative use of steady-flow sensors to determine local stream angles and mean-flow properties, such as fluid density or velocity in arbitrary three-dimensional turbulent flow fields. The second is that associated with the determination of quantitative properties of the unsteady flow. The objective of the present report is to describe efforts, performed under the present subtask, to determine which instruments and sensors are best suited to the AFWL requirements, to provide calibration of this selected instrumentation and, finally, to develop data reduction techniques and demonstrate their use in a practical environment.

NOMENCLATURE

a_w	=	overheat parameter, $(R_w - R_r)/R_r$
E	=	voltage
M	=	Mach number
p	=	pressure
R	=	resistance
$R_{\rho uv}$	=	mass flux crosstream - velocity correlation coefficient
S	=	sensor sensitivity coefficient
u	=	streamwise velocity component
v	=	crosstream velocity component
y	=	coordinate normal to surface
α	=	angle of attack
β	=	side slip angle
γ	=	ratio of specific heats
δ	=	boundary-layer thickness
ρ	=	fluid density
τ	=	shear stress $\bar{\rho}\ \overline{u'v'}$
θ	=	total flow angle
$\langle ( ) \rangle$	=	standard deviation (rms) of quantity

<u>Subscripts</u>

A	=	sensor A (positive v sensitivity)
B	=	sensor B (negative v sensitivity)
e	=	edge conditions
ℓ	=	local conditions in boundary or shear layer
r	=	recovery conditions
u	=	streamwise velocity
v	=	streamnormal velocity

w	=	wire conditions
ρ	=	density
ρu	=	mass flux

Superscripts

$( )'$	=	fluctuation quantity
$(\bar{})$	=	time-averaged quantity

SECTION II SELECTION OF AERODYNAMIC INSTRUMENTATION

Research into previously used instrumentation for determining mean-flow properties of three-dimensional flow fields indicated that either 5-hole or 7-hole pressure probes on continuously-driven probe positioning devices are best suited to the present wind tunnel and flight programs envisioned under current AFWL efforts. The choice between 5-hole and 7-hole pressure-probe technology is driven by the maximum expected flow angularity within the flow field. Generally, Pitot-static probe combinations which involve a 2-hole probe are valid for local flow angles up to 10 deg. This limitation can be significantly extended by the use of 5-hole probes and calibrations developed by the USAF Academy. These 5-hole probes are considered valid in flows whose flow angularity with respect to the probe access is less than about 30-35 deg. Recent USAF Academy calibration and use of 7-hole probes have demonstrated their validity for flow angles up to 80 deg. For most of the flow fields envisioned in AFWL applications, flow angularities of less than 30 deg. are expected. Thus, it appears evident that the 5-hole probe is best suited for purposes of the present application. Ease in calibrating and signal interpretation from the 5-hole probes compared with that of the 7-hole probe add to the justification for considering only the 5-hole probe.

A background review of two primary measurement systems known to be useable in turbulent flow fields for quantitative

diagnostics of unsteady flow properties are the hot-wire or hot-film anemometer system, or the multi-component laser velocimeter system to measure mutually orthogonal components of the velocity vector. With either of these systems, there exists a wide range of flows for which today's use of these systems is, at best, extremely difficult. The laser velocimeter has been used extensively to measure fluctuating velocities in two-dimensional subsonic, transonic and supersonic flow fields. However, in three-dimensional flow fields, the multi-component nature of the system makes it difficult to use in practice. Where applicable, the laser velocimeter is extremely useful in that it is a non-intrusive device and can be used in relatively complicated turbulent flow fields, including flow fields with separation. Laser velocimetry, however, can be time consuming in high speed flows and particularly those in those experiments conducted in the atmosphere where low particle arrival rates are typical. In AFWL applications, correlation volumes of the unsteady flow are required to assess optical propagation characteristics. As of today, there has not been a demonstrated laser velocimeter system capable of obtaining the required correlation lengths in each of the mutually orthogonal directions.

The classical instrumentation system used for measuring unsteady flows is the hot-wire or hot-film anemometer. This system gives an analog signal that can be used to obtain data very quickly in most flows, and data for which real time or post-experiment correlations can be performed between various sensors

in order to establish the required correlation lengths. Hot-wire anemometry has been used extensively in previous AFWL wind tunnel and flight experiments involving two-dimensional, or nearly two-dimensional, flow fields. Relatively simple data gathering and interpretation techniques have been used to obtain quantitative data for use in optical propagation calculations. Techniques developed by the contractor for signal interpretation in flow fields ranging from subsonic to supersonic speeds have shown the usefulness of this system for making measurements in turbulent flow fields. Thus, the hot-wire or hot-film anemometer system has been chosen as the primary unsteady data technique to be used and developed under the present subtask.

SECTION III INSTRUMENTATION REQUIREMENTS

Both the mean-flow and unsteady-flow instrumentation chosen for calibration and use in the present subtask are required to operate over a range of Mach numbers from near zero to approximately 1.5. In wind-tunnel environments, Reynolds numbers up to approximately 15×10^6/m are encountered, while in flight, they lower to about 6×10^6/m. The mean-flow instrumentation must yield the local Mach number and local flow angle relative to the probe axis at any point within the flow field. These Mach number and flow angle data are required for quantitative interpretation of the hot-film signals as discussed in the instrumentation section, as well as defining the mean-flow properties.

The unsteady instrumentation must be calibrated over approximately the same operating range and must be capable of yielding information useful in determining optical propagation characteristics and in determining general aerodynamic flow field behavior for use in modeling in support of computational techniques. For use in turbulence modeling for computational studies, orthogonal component correlations are required in order to establish the unsteady momentum transport terms required in the closure of the Navier-Stokes equations. To this end, instrumentation must be chosen, calibrated and demonstrated which will allow orthogonal velocity vector components to be correlated and their correlation determined as a function of position within the flow field.

A classical instrumentation system for measuring these correlation products (also known as the Reynolds shear stresses) has been the hot-wire anemometer. One difficulty arises in using fine-wire (typically Tungsten wires of the order of 5 μm) instrumentation is the limited lifetime of the sensors in highly turbulent or high dynamic-pressure flow fields. In past AFWL flight and wind-tunnel experiments, AFWL and contractor personnel have demonstrated the use of thin-film sensors. Films usually consisting of nickle deposited on quartz rods have been shown to be much more durable, particularly in the flight environments. An x-array sensor, using this thin-film technique, would have a use similar to the previously used x-array of wires. Recently, sensors made by depositing two electrically independent films onto a single quartz rod has become commercially available. The probe has been used previously in water and Sanborn and Seegmiller (Ref 1) have extended the use of the split-film sensors in gas at M=0.22. These film sensors will meet the requirements for proposed AFWL aerodynamic studies.

The 5-hole pressure probe design chosen for in use in the present study is that as used by Raman (Ref 2) in previous AFWL and NASA experimental programs. A sketch of the probe used in Reference 2 is shown in Figure 1. The size of the probe tip is required to be small so that the overall probe is of relatively small size in comparison with flow fields to be measured. Since these probes are not available commercially, two representative 5-hole probe tips were manufactured by General Dynamics, Albuquerque. Each sensor must be constructed and then individually cali-

brated over the range of flow variables to be encountered.

Sensors for use in unsteady flow experiments were based on the film technology as discussed above and were chosen to be a split-film sensor DISA model 55R58 and an x-array sensor DISA model 55R51. The DISA sensors were chosen for compatibility with existing AFWL sensor holders and anemometry.

SECTION IV CALIBRATION AND SIGNAL INTERPRETATION

The calibration of two 5-hole pressure probes, the split-film sensors, and an attempted calibration of an x-wire array were carried out in July 1982 at the USAF Academy in Colorado Springs by contractor and AFWL personnel. The calibration techniques for the 5-hole probe relied heavily on the previous work (Ref 2) done by Raman, who also calibrated instrumentation at the Academy. The coefficients relating the pressures to flow angle and local flow parameters are given below. A sketch of the arrangement of the hole numbering system is also given in Figure 2. The α and β terms refer to angle of attack and angle of sideslip, respectively, and are determined from the differences in pressure readings across the probe in the two orthogonal directions. The total pressure is assumed for all cases to be equal to the reading p_1, since angles in the calibration did not exceed approximately 15 deg.

$$p_{t,\ell} = p_1$$

$$p_{ave} = \frac{p_2+p_3+p_4+p_5}{4}$$

$$C_\alpha = \frac{p_3-p_5}{p_1-p_{ave}}$$

$$C_\beta = \frac{p_4-p_2}{p_1-p_{ave}}$$

Curve fits of the coefficients for α and β were performed by AFWL personnel for the 5-hole probe number 2, which was used in the calibration checkout experiment. Cubic curves were fitted

to the data for α and β and are given in Equations 1 and 2.

$$\alpha = 3.69 + 19.02\ C_\alpha - .81C_\alpha^2 - 10.15\ C_\alpha^3 \quad (1)$$

$$\beta = 2.19 - 11.62\ C_\beta + 1.23\ C_\beta^2 + 6.33\ C_\beta^3 \quad (2)$$

The overall angle, θ is given by Equation 3.

$$\theta = \tan^{-1}\left[(\sin^2\alpha + \tan^2\beta)^{\frac{1}{2}}/\cos\alpha\right] \quad (3)$$

Pressure measurements of the five pressures will thus yield the local flow angularity with respect to the probe axis.

Local flow parameters, such as Mach number, velocity or density, are determined by first determining the indicated Mach number S_ℓ as given by Equation 4.

$$S_\ell = \left\{\left[\left(\frac{p_1}{p_{ave}}\right)^{2/7} - 1\right] * 5\right\}^{1/2} \quad (4)$$

The Mach number coefficient as determined from the calibrations is only slightly affected by overall flow angle as shown in Equation 5.

$$C_m = .802 + .002\theta + .000248\theta^2 \quad (5)$$

Where $C_m = M_\ell/S_\ell$

And, finally, Equation 6 allows a determination of the actual local Mach number from the indicated Mach number and calibrated Mach number coefficient.

$$M_\ell = S_\ell\ C_m \quad (6)$$

Equations 7 and 8 give the local density and local velocity in terms of measured flow parameters and the indicated total temperature.

$$\rho_\ell = \frac{2.7\ p_1}{T_t\left(1+\frac{M^2}{5}\right)^{2.5}} \qquad T_t \text{ in } ^\circ R \quad (7)$$

$$\bar{u}_\ell = 49.03\, M_\ell \left(\frac{T_t}{1+\frac{M^2}{5}} \right)^{1/2} \qquad T_t \text{ in } °R \tag{8}$$

For flight conditions, the indicated outside air temperature is read from the aircraft instrumentation system, modified to actual total temperature through the known bulb recovery factor, as indicated in Equation 9.

$$T_t = [1 + .2(M^2]\ OAT \tag{9}$$

The above calibrated coefficients and data reduction procedures are those used in the remainder of the present report. As of the date of this report, open questions remain as to the surety of the calibrations obtained in the July test. Another entry into the Academy tunnel by AFWL personnel in November, 1982, seemed to indicate difficulties with respect to procedures used in both the July and November entries. Future calibration tests are planned.

Calibration of the 5 μm wire array in July was unsuccessful due to wire breakage during the time of tunnel operation. However, six split films were calibrated for angular and mass-flux sensitivity. An example of this direct calibration procedure yielded an overall v sensitivity coefficient from the difference of the voltages of approximately 0.25 per radian. The streamwise mass-flux sensitivity for the split film, as determined for the sum of the voltages, indicates a value of approximately 0.19. This is in good agreement with solid-film sensitivity coefficients as determined in previous wind-tunnel and AFWL flight-test programs. Signal interpretation from the split-film sensor, as well as the x-array film

sensor, is of primary importance and is discussed below.

Because of the late delivery of the x-film array used in the flight experiment, calibrations were not available prior to the flight test. A post-test calibration was performed by contractor and AFWL personnel at the NASA-Ames Research Center from 30 November to 2 December, 1982. A small bench calibration rig was used in contrast to the full scale 2-foot blowdown wind tunnel used at the Academy. Slight differences between calibrations obtained in the small-scale facility and those at the Academy were observed and remain unexplained.

The signal interpretation from the split-film sensor used in this study is of primary importance and is discussed below. There is a strong analogy with signal interpretation procedures used by previous workers using crossed (x-array) wires. The procedures outlined below also rely on the transonic hot-wire anemometry interpretation procedures outlined in Reference 3. In addition, although compressibility effects are explicitly accounted for, total temperature fluctuations are considered negligible in the present analysis. The aircraft skin is very nearly adiabatic and previous measurements using 5 μm wires have shown these fluctuations to be quite small.

For either a split-film or x-array sensor the following general response equation holds for an overheat ratio of at least 0.8 (a_w=0.8) so that total temperature sensitivities are quite small.

$$\frac{E'}{\bar{E}} = \frac{\partial \ln E}{\partial \ln \rho u} \frac{(\rho u)'}{\bar{\rho}\,\bar{u}} \pm \frac{\partial \ln E}{\partial \phi} \frac{v'}{\bar{u}} \qquad (10)$$

$$= S_{\rho u} \frac{(\rho u)'}{\bar{\rho}\,\bar{u}} \pm S_v \frac{v'}{\bar{u}} \qquad (11)$$

Equations 10 and 11 define the logarithmic sensitivity coefficients used throughout this study. They are used because of their simplicity, their insensitivity to changes in sensor resistance with age, and they are largely insensitive to changes in overheat ratio. If A and B refer to the upper and lower halves of the split-film or to each of the films of an x-array sensor, then Equation 11 can be written as

$$\frac{E_A'}{\bar{E}_A} = S_{\rho u_A} \frac{(\rho u)'}{\bar{\rho}\,\bar{u}} + S_{v_A} \frac{v'}{\bar{u}} \qquad (12a)$$

and

$$\frac{E_B'}{\bar{E}_B} = S_{\rho u_B} \frac{(\rho u)'}{\bar{\rho}\,\bar{u}} + S_{v_B} \frac{v'}{\bar{u}} \qquad (12b)$$

or

$$E_A' = \bar{E}_A S_{\rho u_A} \frac{(\rho u)'}{\bar{\rho}\,\bar{u}} + \bar{E}_A S_{v_A} \frac{v'}{\bar{u}} \qquad (13a)$$

and

$$E_B' = \bar{E}_B S_{\rho u_B} \frac{(\rho u)'}{\bar{\rho}\,\bar{u}} + \bar{E}_B S_{v_B} \frac{v'}{\bar{u}} \qquad (13b)$$

The sensitivity coefficients $S_{\rho uA}$, $S_{\rho uB}$, S_{vA} and S_{vB} are required in addition to measurements of E'_A, E'_B, $\bar{E}_A$ and $\bar{E}_B$ to determine the primary data quantities $(\rho u)'$ and v'. During the present study direct calibrations of both the split film and x-array sensors were made to evaluate the sensitivity coefficients. For the split films it was found that

$$S\rho u_A = S\rho u_B = S\rho u = 0.19$$

and

$$Sv_A = -Sv_B = Sv = 0.25$$

over the range of $0.25 \leq M \leq 1.04$

For the two x-array sensors used here, calibration data led to the following values:

Sensor #1 $S\rho u_A = S\rho u_B = S\rho u = 0.22$

and $Sv_A = -Sv_B = Sv = 0.24$

Sensor #2 $S\rho u_A = S\rho u_B = S\rho u = 0.22$

and $Sv_A = -Sv_B = Sv = 0.25$

Noting that the sensitivities are the same for elements A and B in Equation 13 gives

$$E'_A = \bar{E}_A S\rho u \frac{(\rho u)'}{\bar{\rho}\,\bar{u}} + \bar{E}_A Sv \frac{v'}{\bar{u}} \qquad (14a)$$

and

$$E'_B = \bar{E}_B S\rho u \frac{(\rho u)'}{\bar{\rho}\,\bar{u}} - \bar{E}_B Sv \frac{v'}{\bar{u}} \qquad (14b)$$

We now add and subtract Equations 14a and 14b to give

$$E'_A + E'_B = \left(\bar{E}_A + \bar{E}_B\right) S\rho u \frac{(\rho u)'}{\bar{\rho}\,\bar{u}} + \left(\bar{E}_A - \bar{E}_B\right) Sv \frac{v'}{\bar{u}} \qquad (15a)$$

and

$$E'_A - E'_B = \left(\bar{E}_A + \bar{E}_B\right) Sv \frac{v'}{\bar{u}} + \left(\bar{E}_A - \bar{E}_B\right) S\rho u \frac{(\rho u)'}{\bar{\rho}\,\bar{u}} \qquad (15b)$$

We see that if the sensors are operated with $\bar{E}_A = \bar{E}_B$ we have a pair of signals proportional to $(\rho u)'$ and v', respectively, i.e.,

$$E'_A + E'_B = \left(\bar{E}_A + \bar{E}_B\right) S\rho u \frac{(\rho u)'}{\bar{\rho}\,\bar{u}} \tag{16a}$$

and

$$E'_A - E'_B = \left(\bar{E}_A + \bar{E}_B\right) Sv \frac{v'}{\bar{u}} \tag{16b}$$

Voltage outputs from the sensors may be put into sum and difference units to produce the left-hand sides of Equations 16a and 16b, respectively, and averaged to give the rms values as follows

$$\frac{\langle (\rho u)' \rangle}{\bar{\rho}\,\bar{u}} = \frac{\left\langle \left| E'_A + E'_B \right| \right\rangle}{\bar{E}_A + \bar{E}_B} \frac{1}{S\rho u} \tag{17}$$

and

$$\frac{\langle v' \rangle}{\bar{u}} = \frac{\left\langle \left| E'_A - E'_B \right| \right\rangle}{\bar{E}_A + \bar{E}_B} \frac{1}{Sv} \tag{18}$$

Further, voltage outputs corresponding to Equations 16a and 16b may be multiplied and time averaged to give the Reynolds shear stress term

$$\frac{\overline{(\rho u)'v'}}{\bar{\rho}\,\bar{u}} = \frac{\overline{\left(E'_A + E'_B\right)\left(E'_A - E'_B\right)}}{\left(\bar{E}_A + \bar{E}_B\right)^2} \frac{1}{S\rho u} \frac{1}{Sv} \tag{19}$$

From Equation 19 we obtain the Reynolds shear stress from the fluctuating and mean flow data as follows

$$\frac{\overline{(\rho u)'v'}}{\bar{\rho}_e \bar{u}_e^2} = \frac{\overline{(\rho u)'v'}}{\bar{\rho}\,\bar{u}^2} \frac{\bar{\rho}\,\bar{u}^2}{\bar{\rho}_e \bar{u}_e^2}$$

and, for adiabatic flows, we have (Ref 3):

$$\frac{\tau}{\bar{\rho}_e \bar{u}_e^2} = \frac{\bar{\rho}\,\overline{u'v'}}{\bar{\rho}\,\bar{u}_e^2} = \frac{\overline{(\rho u)'v'}}{\bar{\rho}_e \bar{u}_e^2} \frac{Pr_t}{1+(\gamma-1)M^2} \tag{20}$$

A check on the accuracy of signal processing for $\langle v' \rangle$ and $\overline{(\rho u)'v'}$ can be performed by considering the A and B sensor signals independently. From Equation 14, we may consider the mean square of each sensor voltage and write

$$\frac{\overline{E_A'^2}}{\bar{E}_A^2} - \frac{\overline{E_B'^2}}{\bar{E}_B^2} = 4\, S\rho u S v \frac{\overline{(\rho u)'v'}}{\bar{\rho}\,\bar{u}^2} \tag{21}$$

and

$$\frac{\overline{E_A'^2}}{\bar{E}_A^2} + \frac{\overline{E_B'^2}}{\bar{E}_B^2} = 2\, S\rho u^2 \frac{\overline{(\rho u)'^2}}{(\bar{\rho}\,\bar{u})^2} + 2\, Sv^2 \frac{\overline{v'^2}}{\bar{u}^2} \tag{22}$$

SECTION V. RESULTS AND DISCUSSION

The instrumentation and signal interpretation procedures outlined in previous sections were applied in an airborne test environment. The primary data sought in this test were Reynolds shear stress in the 30cm aircraft boundary layer and in a shear layer. Data were obtained using a NKC-135 aircraft over a range of flight conditions give in Table I.

TABLE I

TEST POINTS ACCOMPLISHED FOR

REYNOLDS - SHEAR-STRESS EXPERIMENT

DATE	CONFIGURATION	INSTRUMENTATION	ALTITUDE	M
3 Sep 82	Boundary Layer	5-hole pressure/ split film #1	6,000	.57
			6,000	.32
			11,000	.38
			12,500	.57
			18,000	.57
8 Sep 82			19,000	.45
			29,000	.68
			35,000	.79
			35,000	.57
9 Sep 82		5-hole pressure/ X-film #1	6,000	.32
			19,000	.45
			29,000	.68
			35,000	.79
11 Sep 82	Mid-Fence	5-hole pressure/ X-film #2	6,000	.32
			6,000	.25
			29,000	.68
			35,000	.79
13 Sep 82		5-hole pressure/ split film #1	6,000	.32
			6,000	.25
			29,000	.68
			35,000	.79

The unit Reynolds number was approximately $6x10^6$/m. This gives a length Reynolds number of about $2x10^8$ and a boundary-layer thickness Reynolds number of about $2x10^6$. The shear-layer flow was generated by a 48%-porosity, 15cm-high fence placed 80cm ahead of the measuring station. This aircraft and the flowfield configuration have been used in previous aerodynamic tests (Ref 4). Figure 3 shows the instrumentation location for the boundary layer and shear layer configurations investigated.

Of the entire test matrix, only the selected conditions shown in Table II were analyzed in detail here.

TABLE II

M	Alt, km
0.32	1.8
0.64	8.8
0.71	10.6

The mean-flow velocity profiles are shown for the selected outline in Figure 4. The boundary layer flows (Figure 4a) are recovering from a recent history of acceleration associated with the flow over the upper surface of the aircraft wing. They are not representative of equilibrium, near-zero-pressure-gradient flows. We see that the profile is very full, typical of accelerated, high-Reynolds-number layers. The velocity distributions appear reasonable and, for M=0.64, the data compare reasonably well with those taken with a laser velocimeter in the Cycle II.5 (Ref 4) study. Minor differences could be due to calibration uncertainties or actual differences in the aircraft flow field between the two tests. The mean flow data obtained in the shear

layer (Figure 4b) below a distance of approximately 10cm from the wall were ambiguous due to the very low forward velocity over the probe. Here, the data exhibit a severe departure from those obtained with the laser velocimeter. Data in the outer region were used for interpretation of the fluctuating signals.

The rms fluctuating streamwise mass-flux fluctuations are shown in Figure 5 for the M=0.64 case. Data obtained from the present study by the split-film and x-array film sensors are shown in comparison with each other and with data obtained with a 5 μm wire in Reference 4. As is evident, good agreement between the different sensors is seen throughout the boundary layer. Data from both sensors were interpreted with Equation 8 and the respective calibration constants. The present data are in reasonable agreement with those from Reference 4, giving credence to the present data interpretation technique.

The streamnormal fluctuations for the M=0.64 case are shown in Figure 6. Data for both sensors are shown interpreted from the direct method (Equation 18) and by the difference method (Equation 22). Variations between the data from the two sensors is largest in the outer portion of the layer. In the inner portion, scatter in the data due to signal interpretation method is as large as the difference due to sensor type. A ±10% error band would bracket most of the data.

A similar plot for the Reynolds shear stress term $\overline{(\rho u)'v'}$ for the M=0.64 case is shown in Figure 7. Here, the direct method (Equation 19) is compared with the difference method (Equation 21)

for both the split-film and x-film sensors. The data obtained using Equation 21 appear to exhibit less scatter throughout the boundary layer and will be used for the remaining presentations. Again a ±10% error band would encompass most of the data except very near the surface (y=0) where the x-array sensor data show an unexplained increase in value. The data shown in Figure 7 are not usable directly in turbulence modeling; however, the correlation coefficient and the Reynolds stress $\tau = \bar{\rho}\ \overline{u'v'}$ are useful and may be obtained from the data presented above. The correlation coefficient for the M=0.64 case is shown in Figure 8. The data exhibit up to ±20% scatter but are generally in the range of -0.35 to -0.55, typical of boundary layer flows.

Figure 9 shows the Reynolds shear stress data for the two sensors. A calculated shear stress based on mean-velocity gradient and the measured correlation lengths from the study of Reference 4 is also shown for comparison. This curve was calculated from a mixing length approach

$$\frac{\bar{\rho}\ \overline{u'v'}}{\rho_e u_e^2} = -\frac{\bar{\rho}\ \ell^2 \left(\frac{\partial u}{\partial y}\right)^2}{\rho_e u_e^2}$$

where the mixing length, ℓ, is taken to be the integral scale (correlation) length found in Reference 4. The data are interpreted from Equation 20 with Pr_t=1.0 and the mean flow data for local Mach number. General agreement with the measured and calculated data is seen for this case.

Streamwise and streamnormal fluctuations are shown in Figures 10 and 11 at the two other Mach numbers of 0.34 and 0.71. General agreement between the two sensors is shown over the range of Mach

numbers. A quantitative difference in the distribution of streamwise fluctuation levels is seen between the M=0.34 and 0.71 flows. The higher Mach number case exhibits an extensive region of nearly constant intensity while a monotonic decrease is shown with increasing y at the lower Mach number. This quantitative difference is also strongly reflected in the Reynolds shear stress data shown in Figures 12 and 13 for the two Mach numbers. Both sensors are capable of resolving these differences as is shown by the good agreement between them for each of the flows.

To demonstrate the use of the split-film and x-array sensors in another flow, data taken in the shear layer at M=0.64 are shown in Figures 14 and 15. The data for streamwise fluctuations indicate a general agreement between the two sensors and those taken with the 5 μm wire. There is a ±15% scatter in these data, although one must keep in mind the generally unsteady nature of this flow field and the rather large fluctuation levels observed. The Reynolds shear stress data shown in Figure 15 also show a rather large uncertainty between the sensors. Here we should note that the shear stress level is about an order of magnitude larger than shown for the boundary layer flows. Even this ±25% data would be considered useful in turbulence modeling for such a highly turbulent environment.

SECTION VI. CONCLUDING REMARKS

Mean and fluctuating flow data have been obtained at high Reynolds numbers in a boundary layer and shear layer generated on the fuselage of a high subsonic Mach number aircraft. These data were obtained with mean- and fluctuating-flow instrumentation for measuring the turbulent transport properties. This study provides instrumentation verification in a large scale flow so that this instrumentation can be used in smaller scale wind-tunnel environments. The instrumentation chosen for use in the present study for use in measuring Reynolds shear stress are the classical x-array of orthogonal sensors and the newer split-film probe. Results of the present study indicate good agreement between the x-array and split-film sensors for streamwise, streamnormal and turbulent shear stress terms.

SECTION VII. REFERENCES

1. Sandborn, V.A. and Seegmiller, H.L., "Evaluation of Mean and Turbulent Velocity Measurements in Subsonic Accelerated Boundary Layers.", NASA TM X-62,488, March, 1976.

2. Raman, K.R., "Aerodynamic Measurements Concerned with a Turret Model," Final Report Contract No. NAS 2-10579, NASA Ames Research Center, 1980.

3. Horstman, C.C. and Rose, W.C., "Hot-Wire Anemometry in Transonic Flow," AIAA Journal Vol 15, March, 1977, pp 395-401.

4. Rose, W.C., Johnson, D.A. and Otten, L.J., "Application of Hot-Wire Anemometry and Laser Velocimetry to In-Flight Measurement of Turbulent Flow Properties," AIAA Paper 78-825, 10th Aerodyanmics Testing Conference, San Diego, CA, April, 1978.

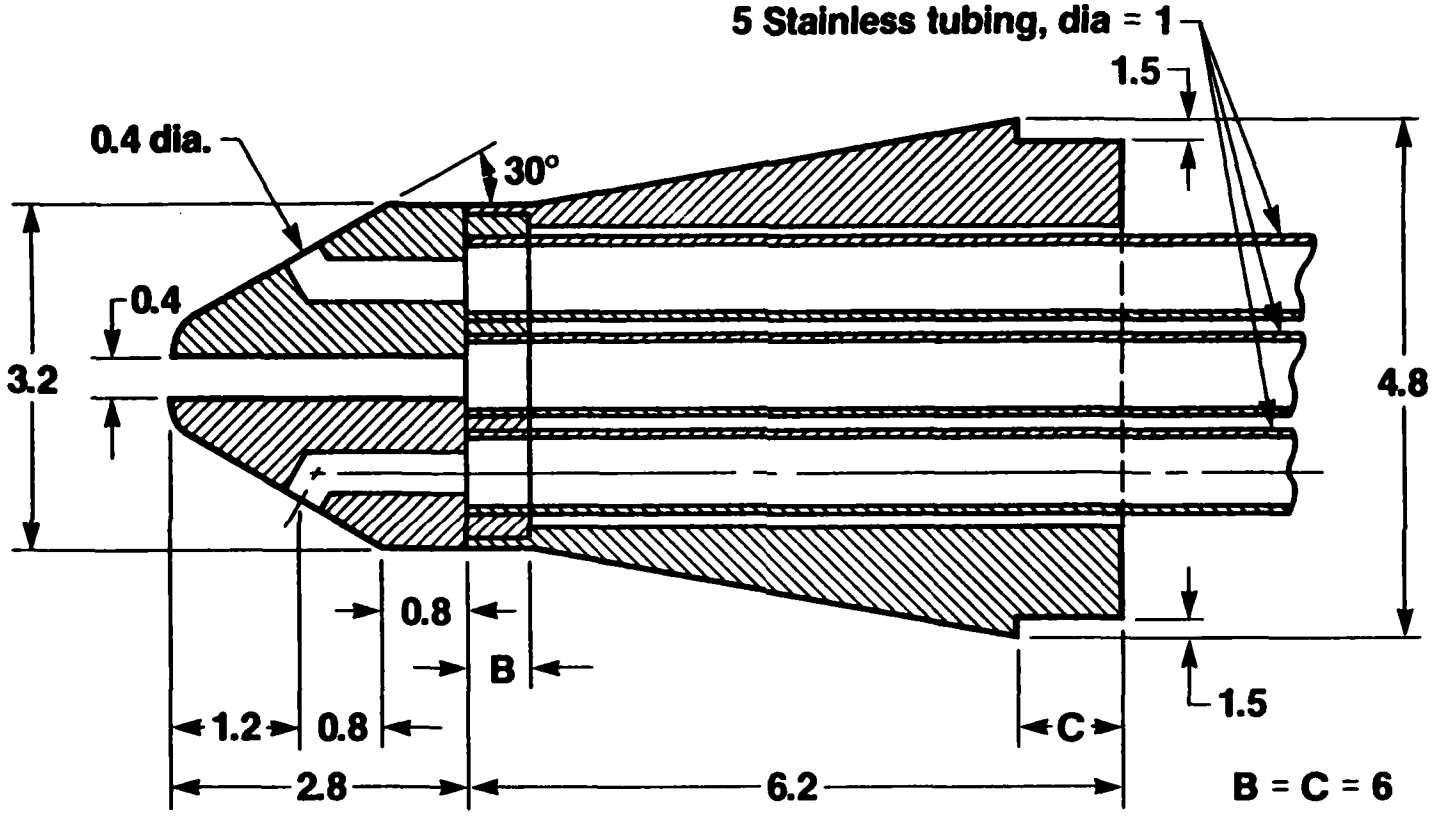

Note: All dimensions are given in millimeters.

Figure 1. Construction details for 5-hole conical-tipped pressure probe.

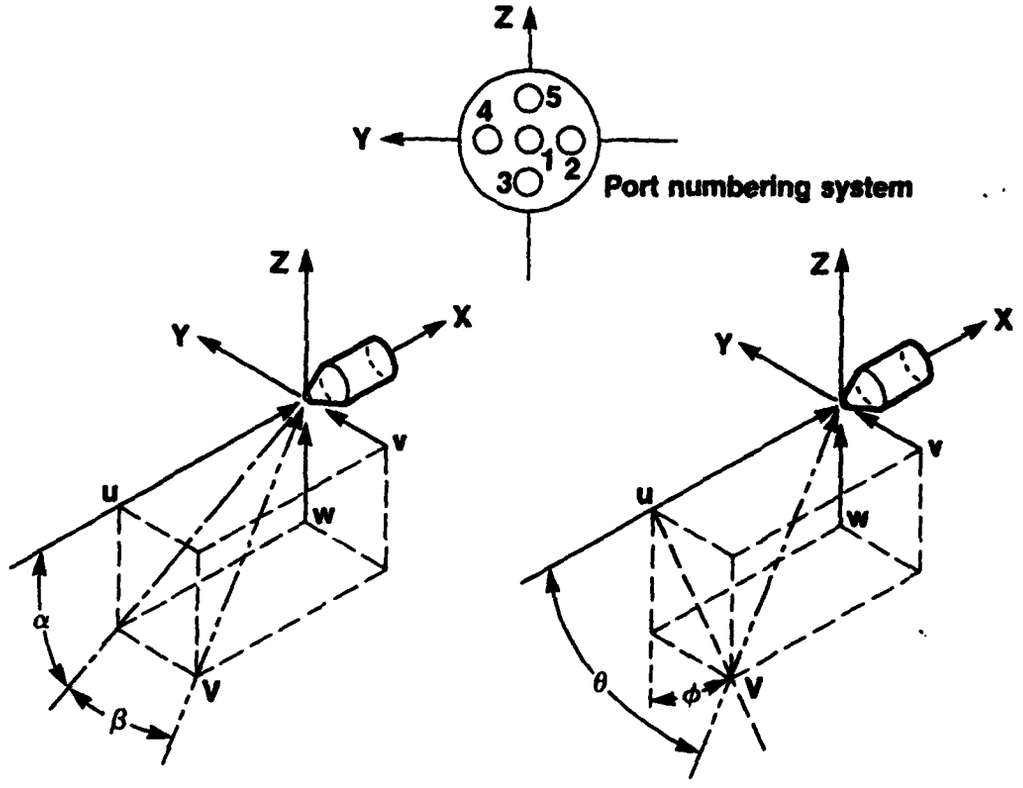

$u = V\cos\alpha\cos\beta$
$v = V\sin\beta$
$w = V\sin\alpha\cos\beta$

$u = V\cos\theta$
$v = V\sin\theta\sin\phi$
$w = V\sin\theta\cos\phi$

$$\sin\alpha = \sin\theta\cos\phi / \cos\beta$$
$$\sin\beta = \sin\theta\sin\phi$$
$$\tan\theta = (\sin^2\alpha + \tan^2\beta)^{1/2} / \cos\alpha$$

Figure 2. Nomenclature and numbering system for 5-hole pressure probe.

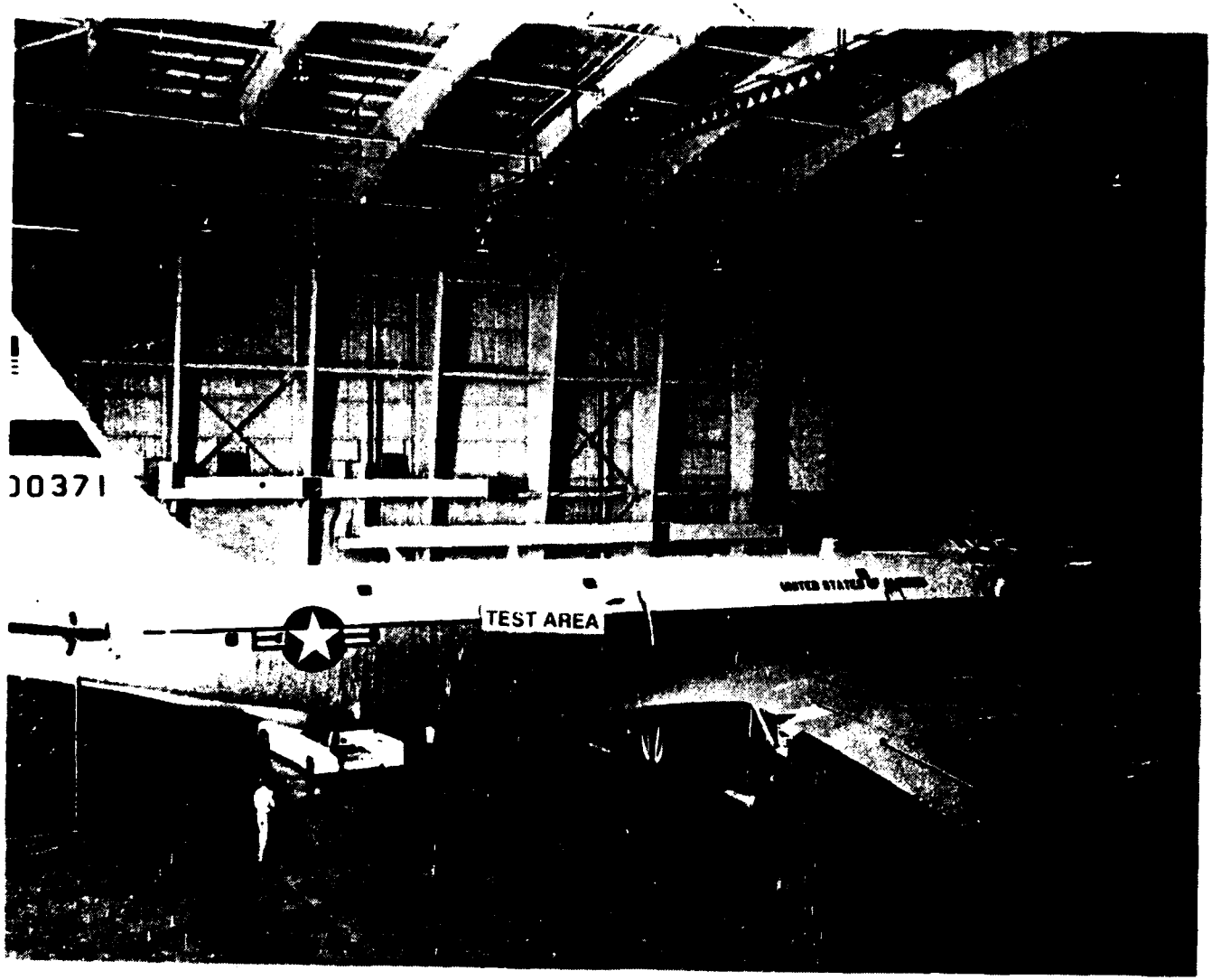

a) Overall view of aircraft.

Figure 3. Photographs of instrumentation installations and flow configurations.

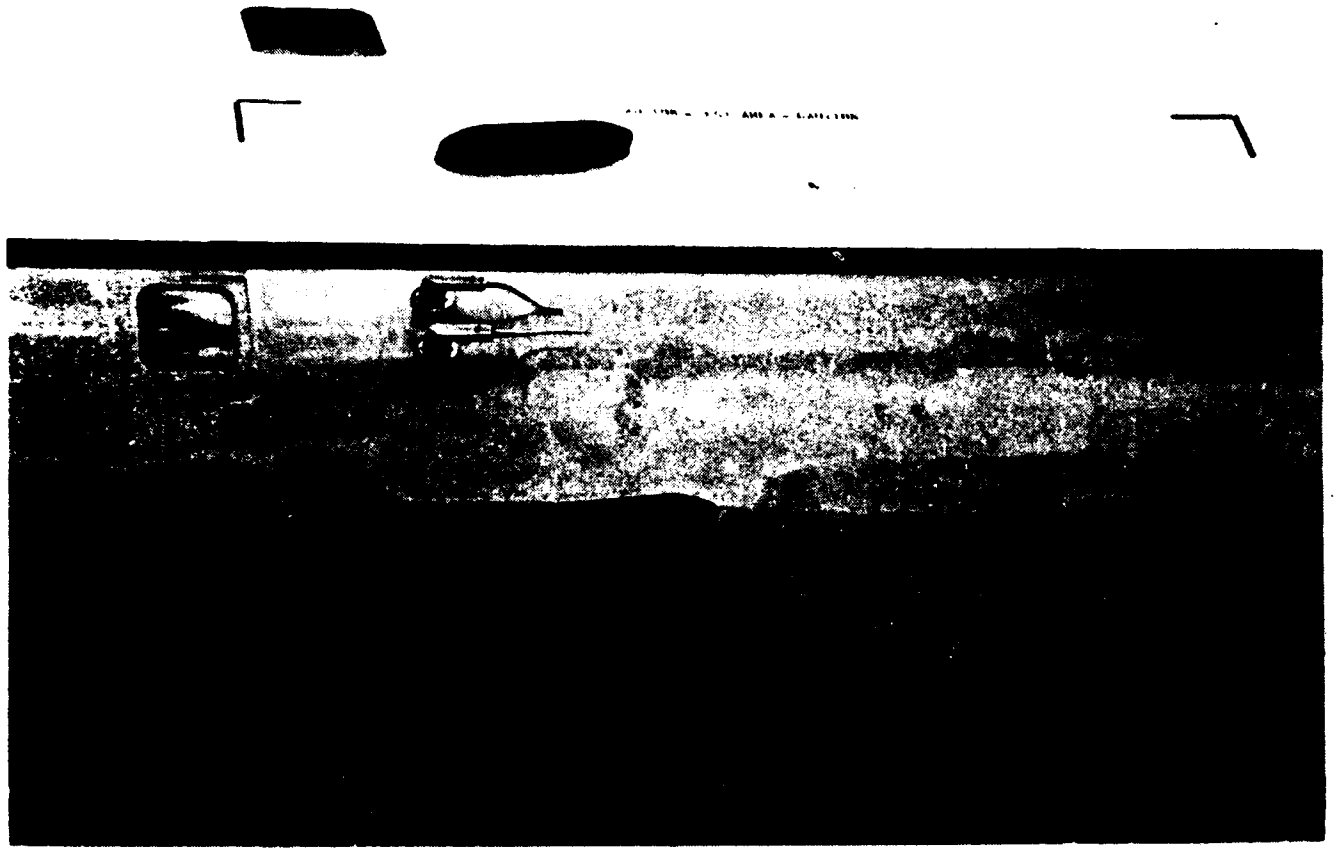

b) Boundary layer configuration.

Figure 3. Continued.

c) Porous fence configuration.

Figure 3. Concluded.

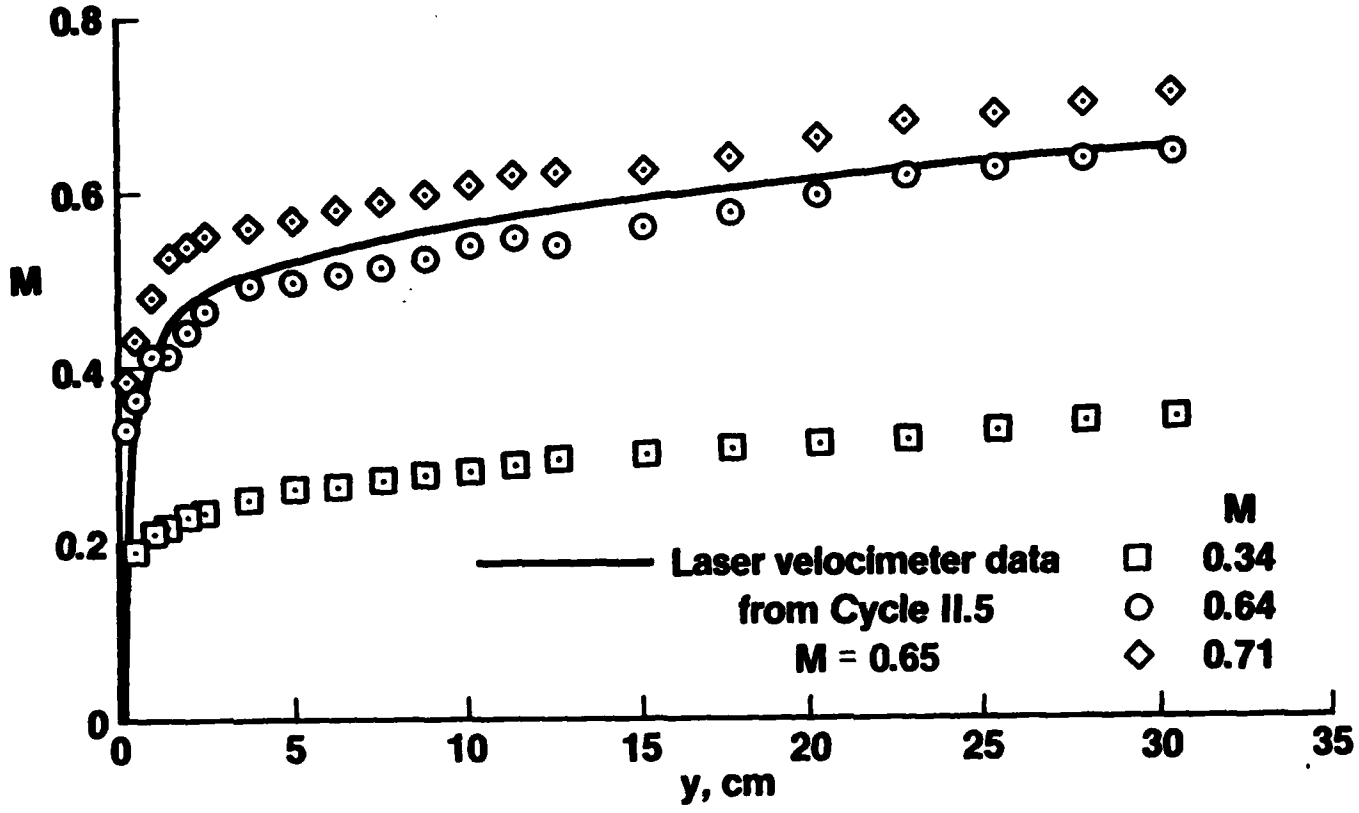

a) Boundary layer cases.

Figure 4. Mean-Flow Mach number profiles.

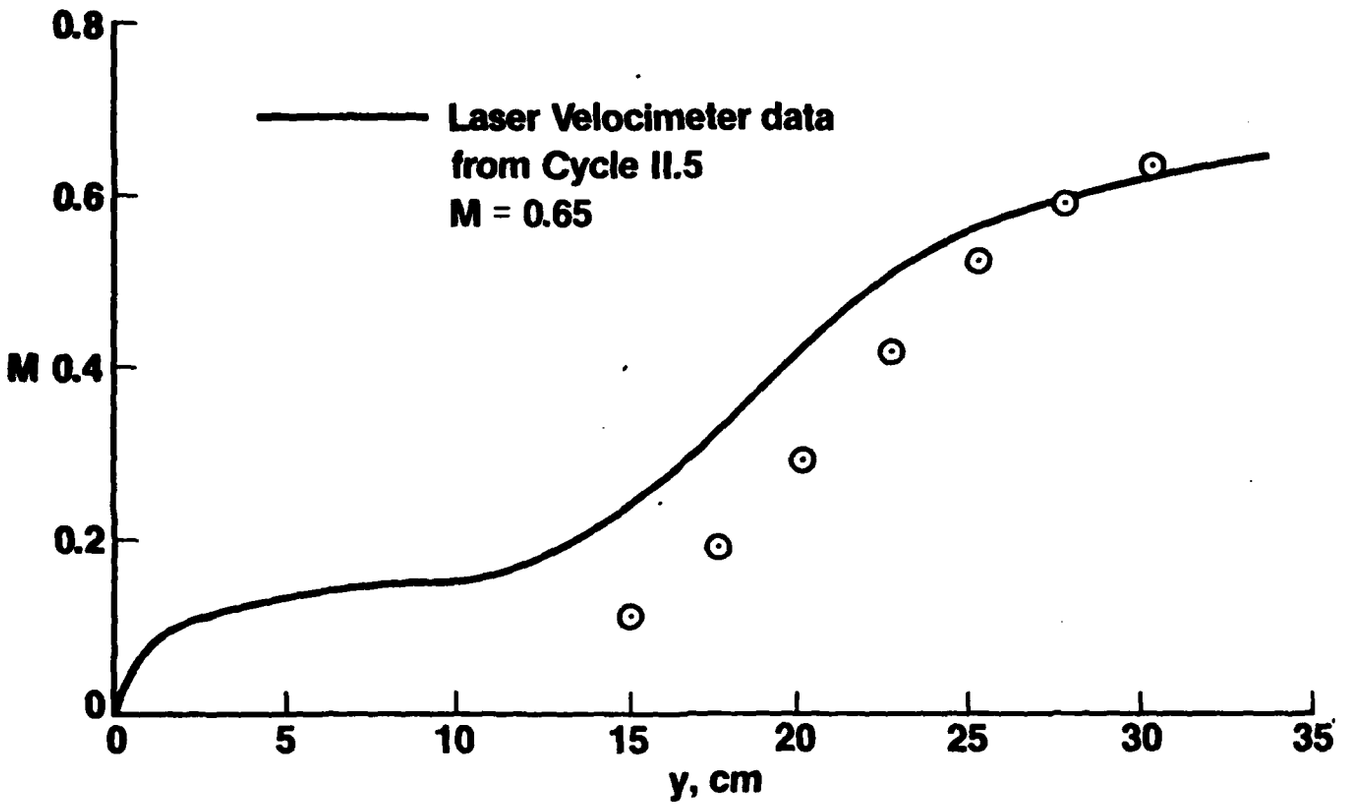

b) Shear layer case.

Figure 4. Mean-Flow Mach number profiles.

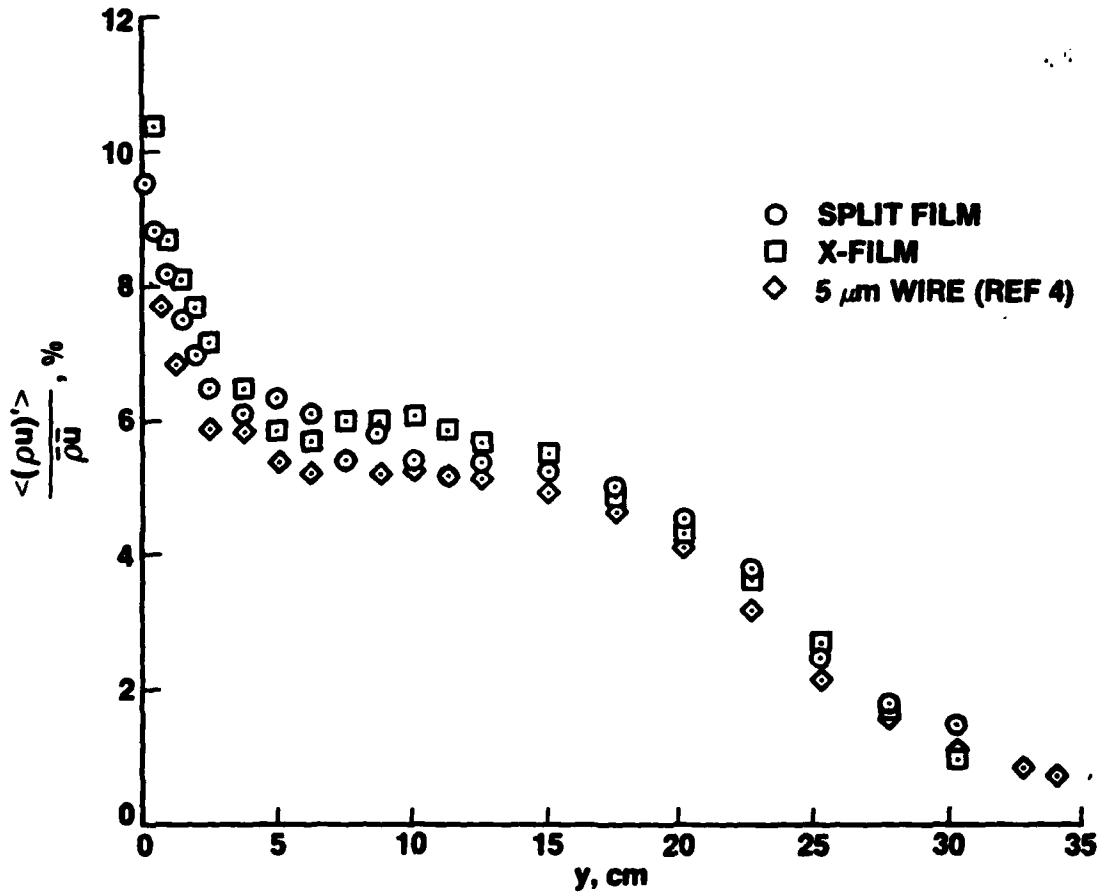

Figure 5. Streamwise fluctuations for boundary layer; M = 0.64.

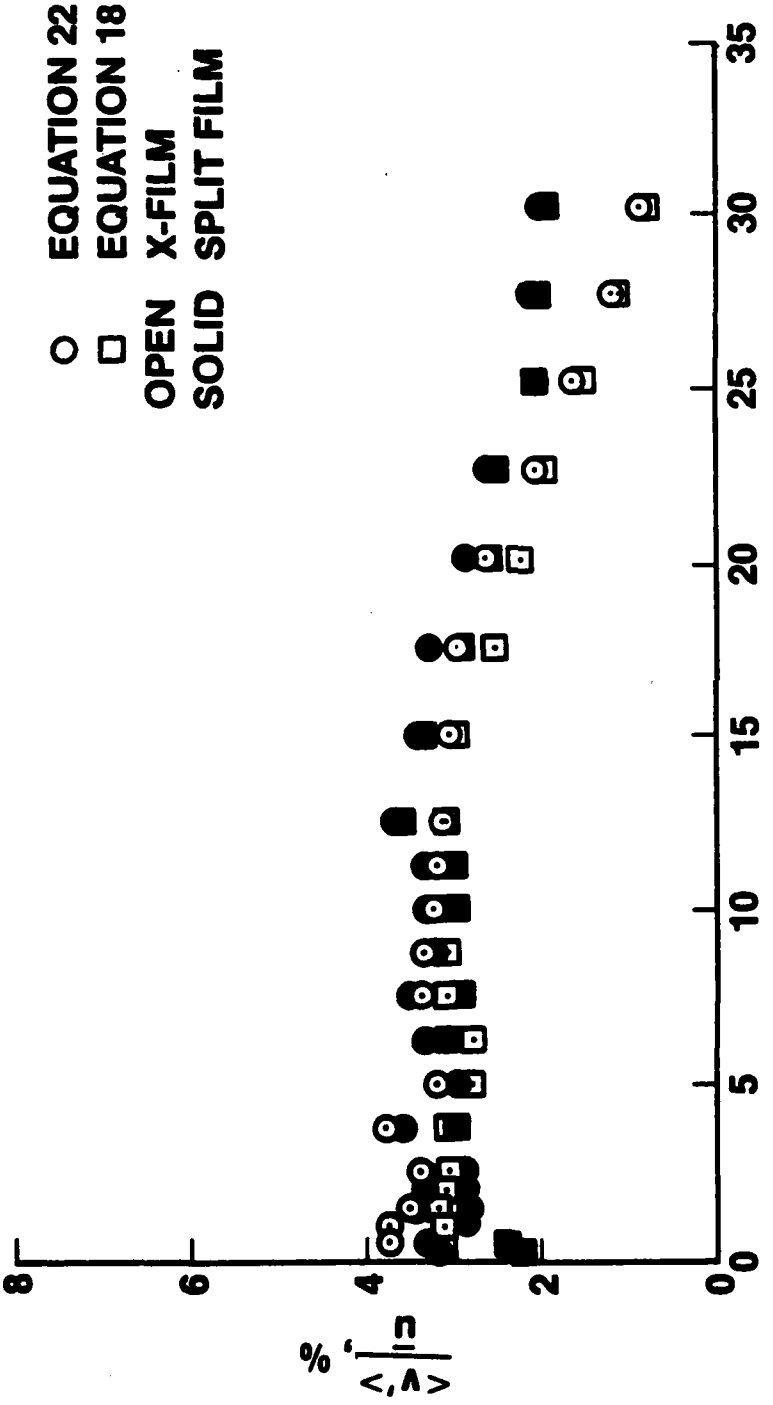

Figure 6. Comparison of stream normal fluctuations obtained from Equations 18 and 22 for boundary layer; M = 0.64.

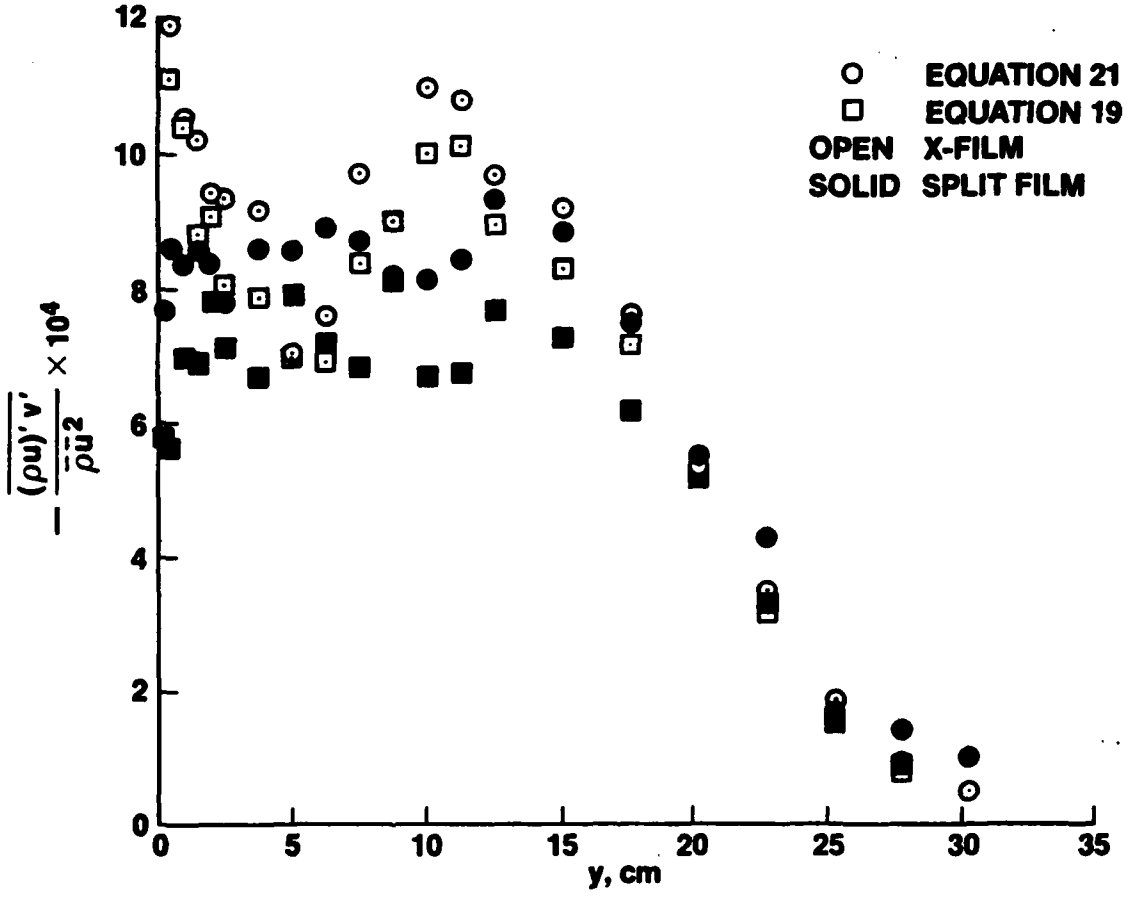

Figure 7. Comparison of Reynolds-stress term obtained from Equations 19 and 21 for boundary layer; M = 0.64.

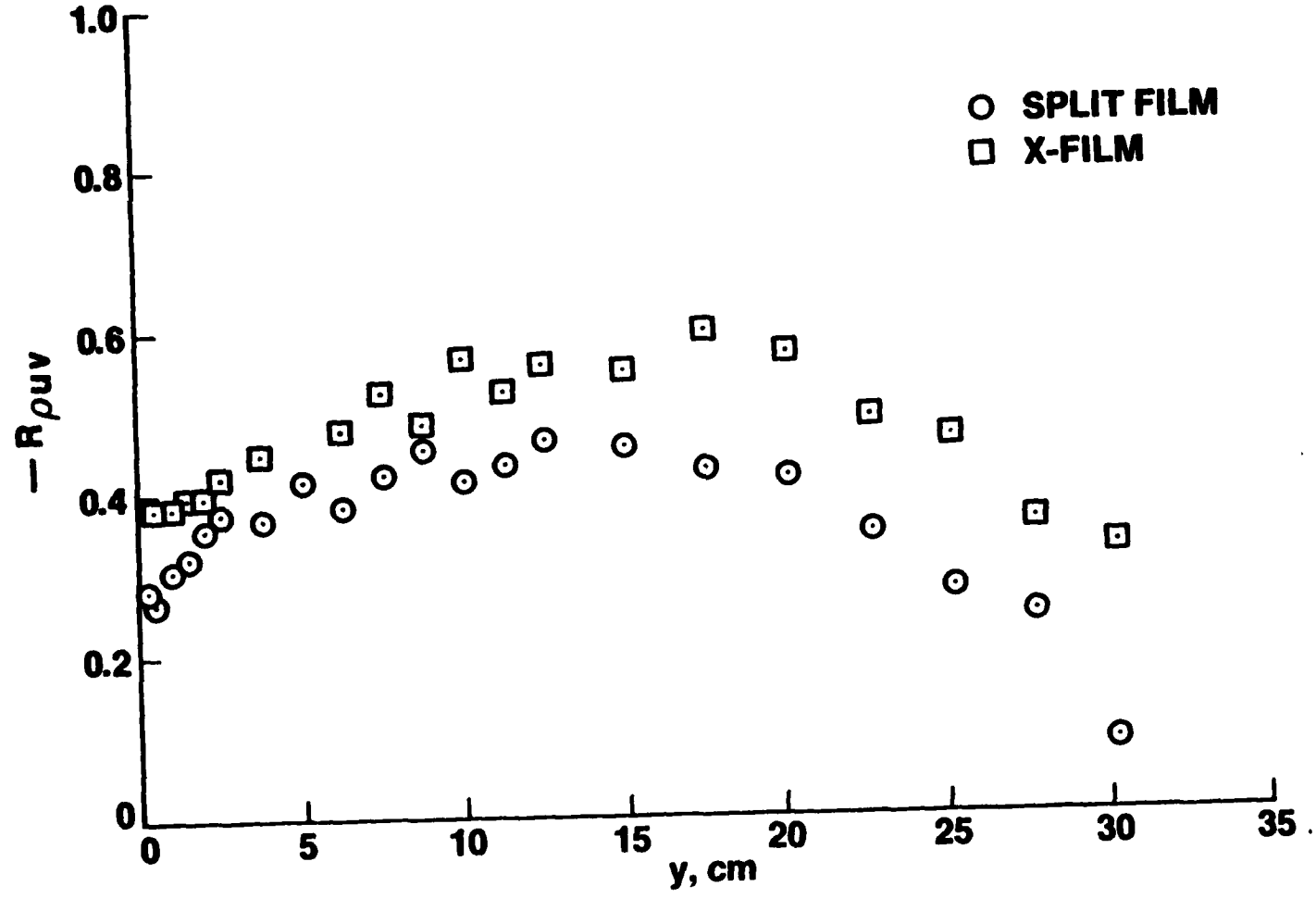

Figure 8. Variation of correlation coefficient for bounfary layer; M = 0.64.

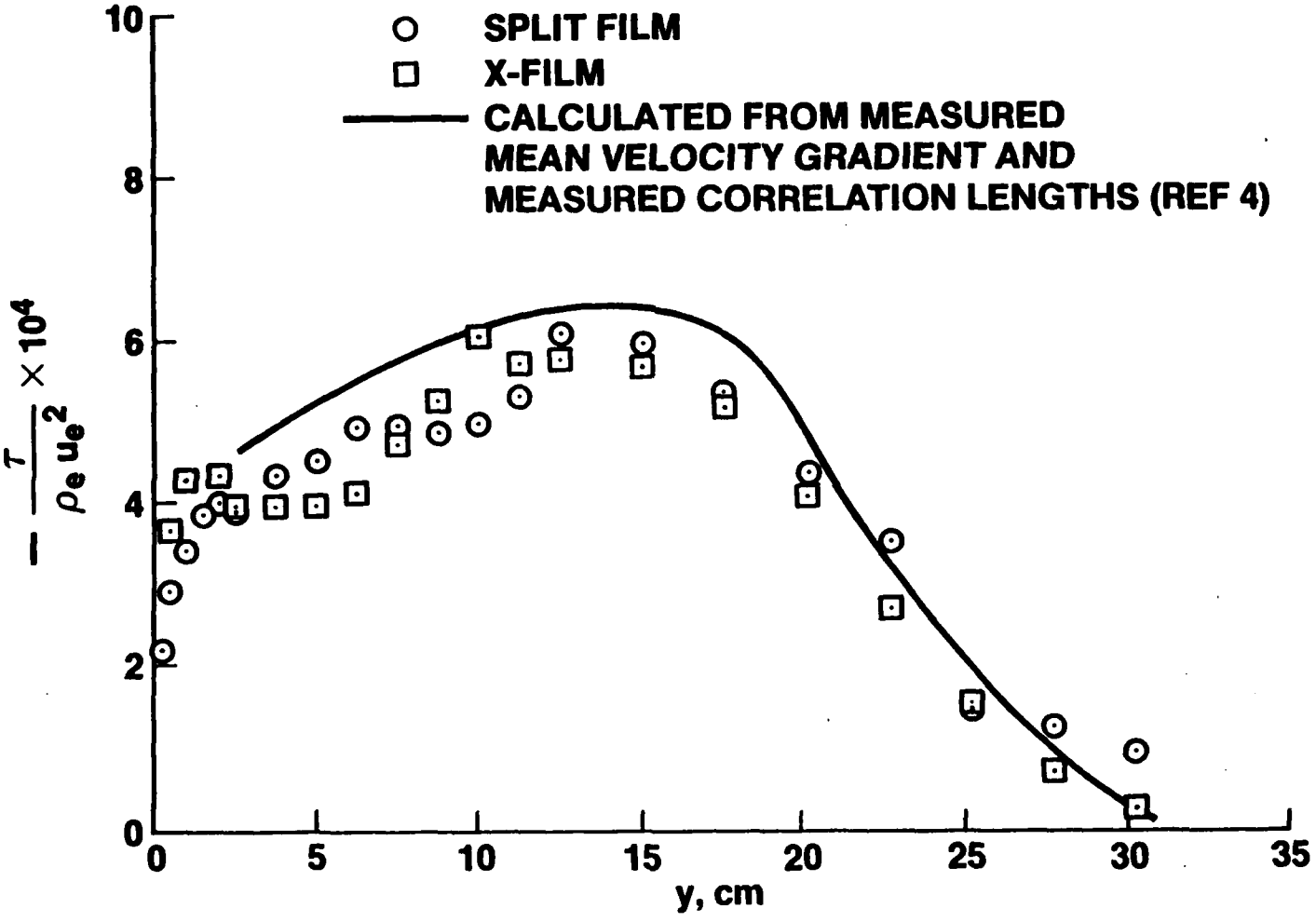

Figure 9. Reynolds shear stress for boundary layer; M = 0.64.

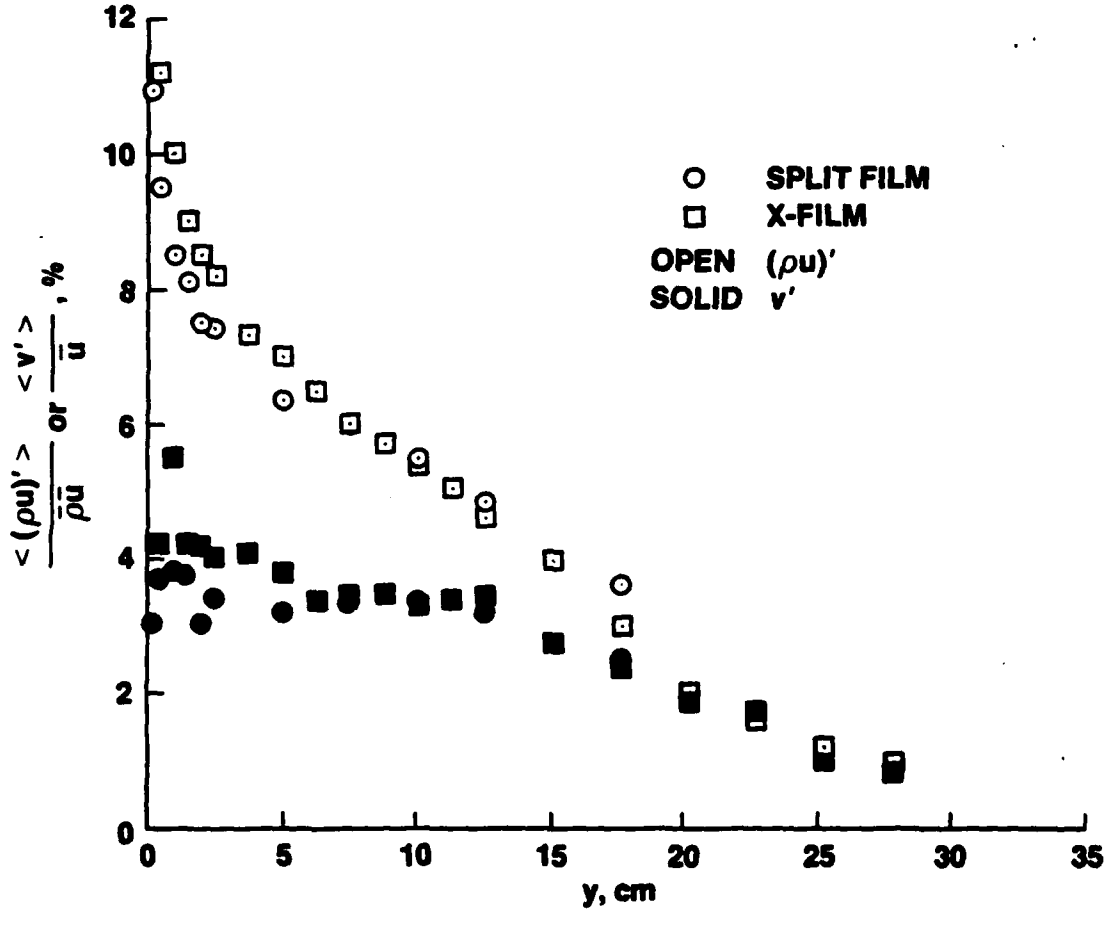

Figure 10. Streamwise and streamnormal fluctuations for boundary layer; M = 0.34.

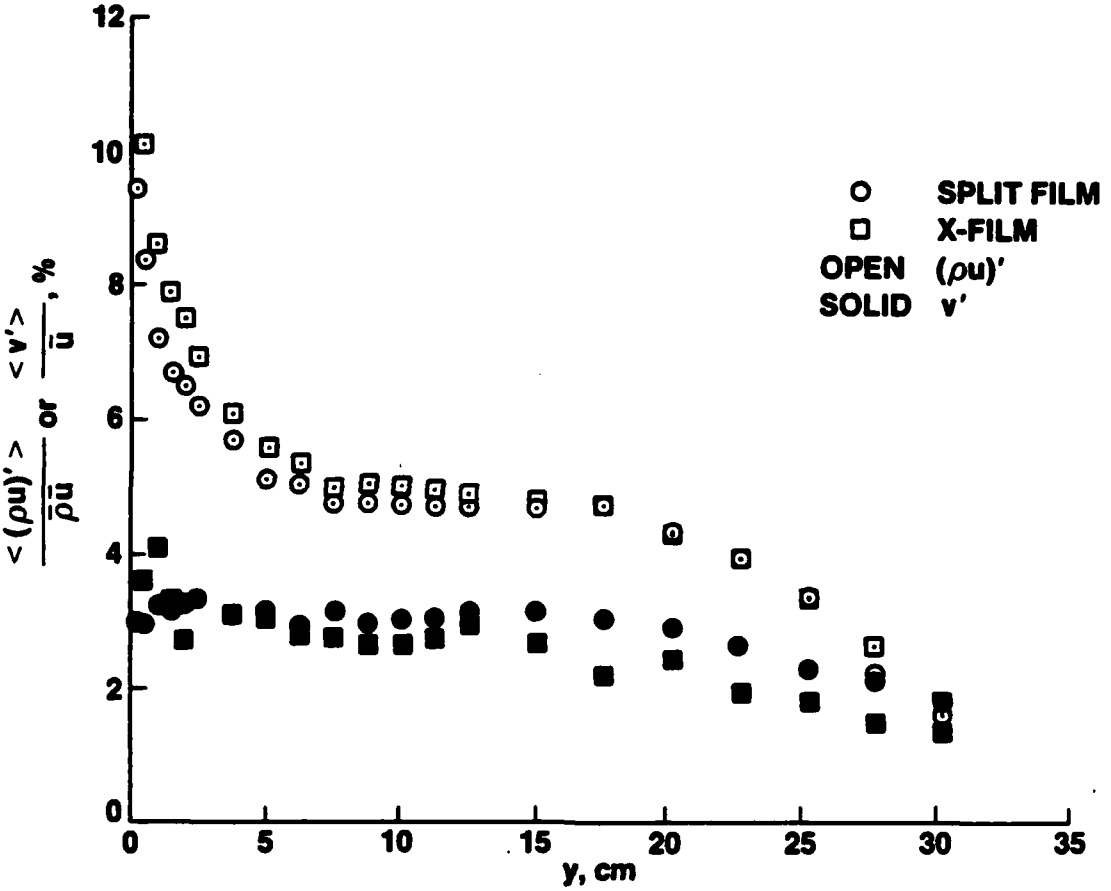

Figure 11. Streamwise and streamnormal fluctuations for boundary layer; M = 0.71.

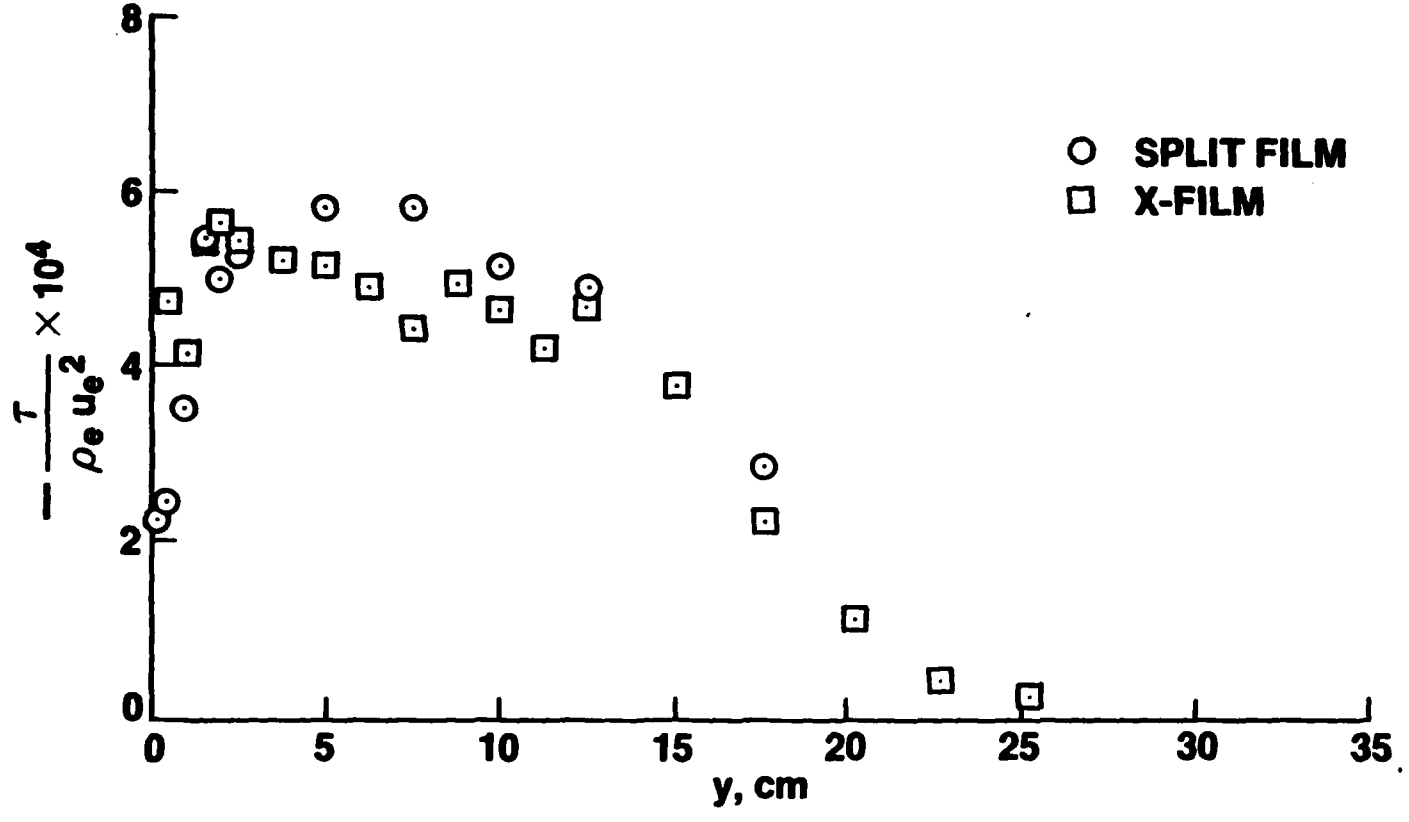

Figure 12. Reynolds shear stress for boundary layer; M = 0.34.

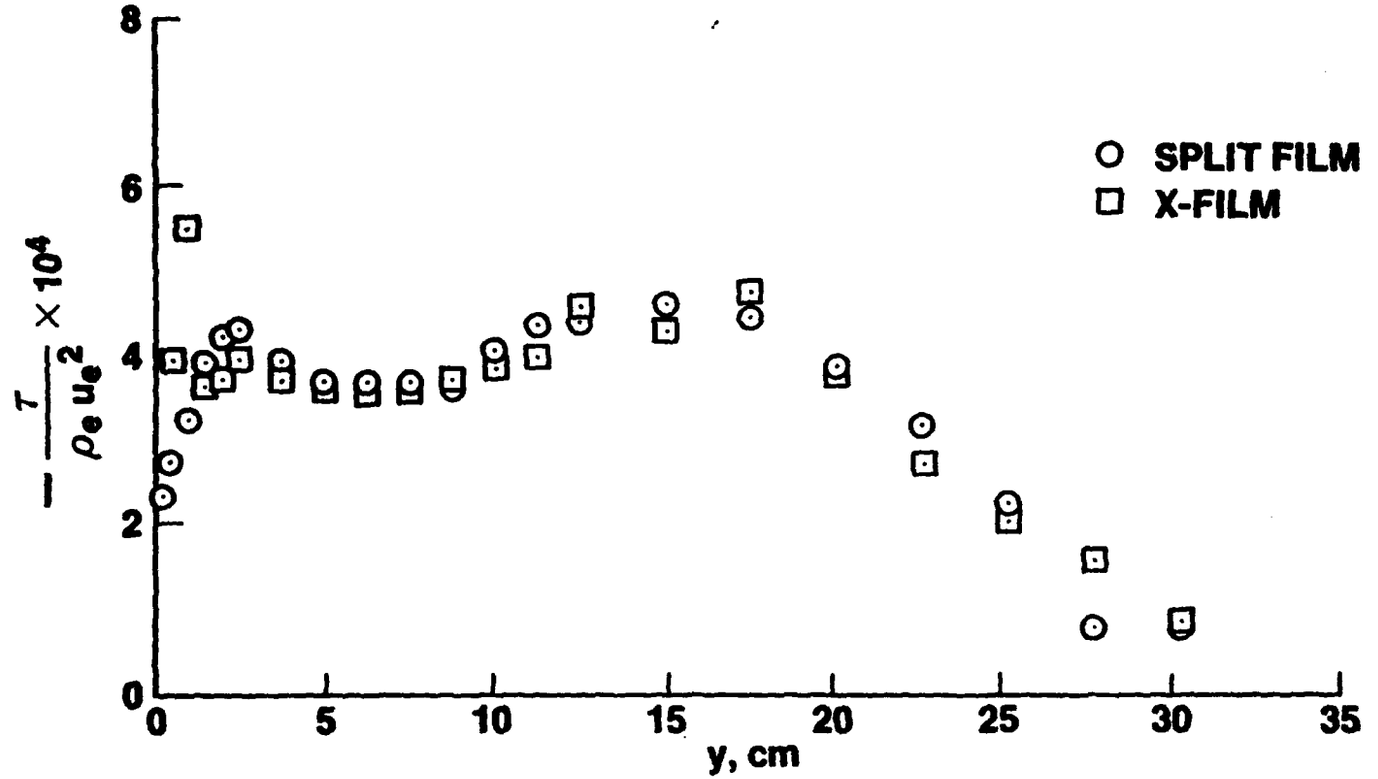

Figure 13. Reynolds shear stress for boundary layer; M = 0.71.

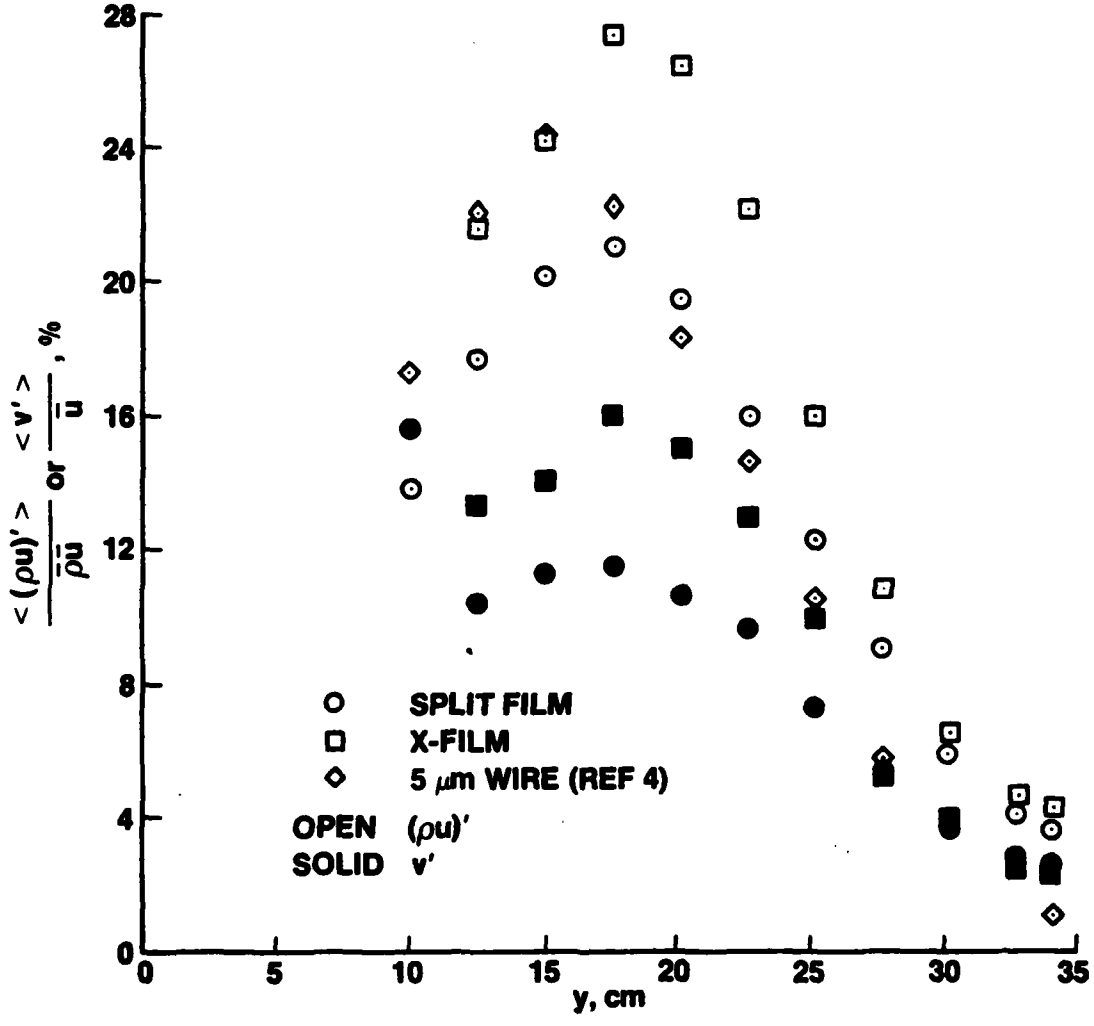

Figure 14. Streamwise and streamnormal fluctuations for shear layer; M = 0.64.

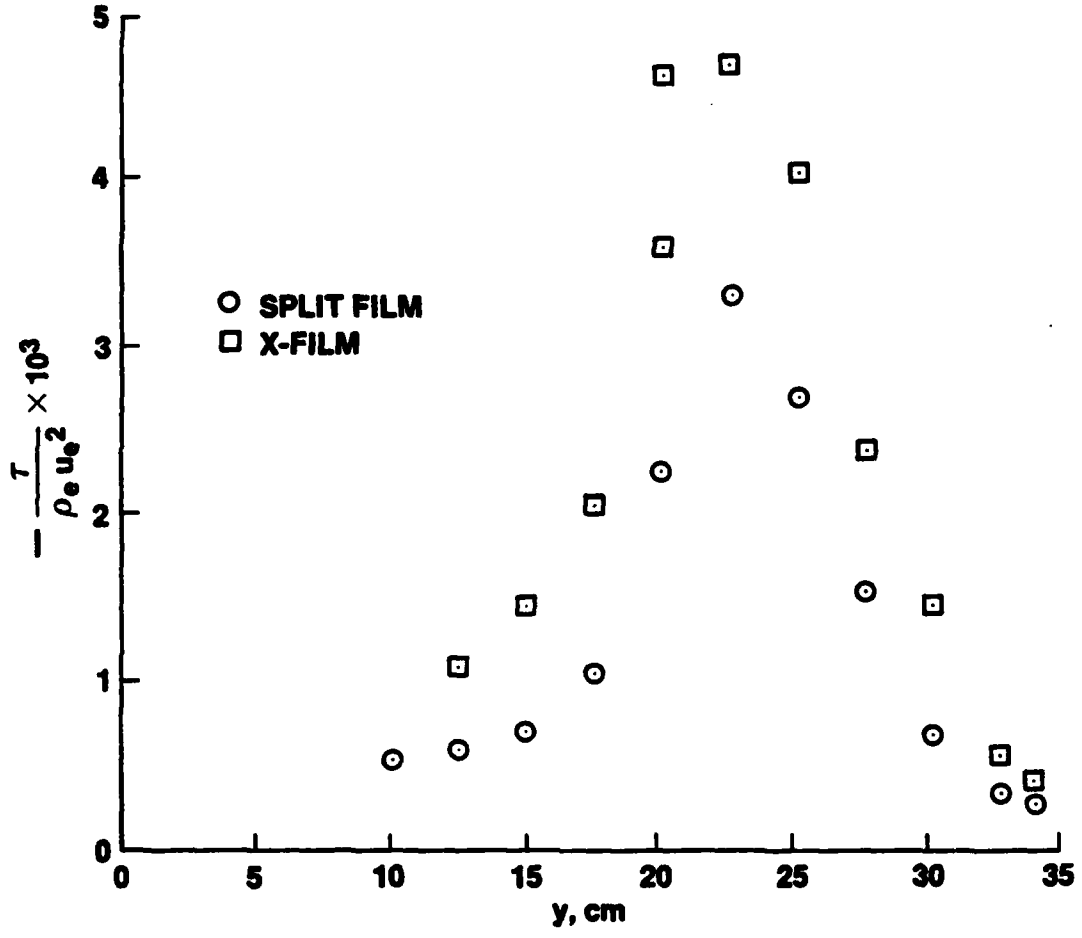

Figure 15. Reynolds shear stress for shear layer; M = 0.64.

D

E

ED

84

C